

## Doubly ionized lanthanum as a qubit candidate for quantum networks

S. Olmschenk <sup>\*</sup>*Department of Physics and Astronomy, Denison University, Granville, Ohio 43023, USA* (Received 4 September 2021; revised 6 March 2022; accepted 7 March 2022; published 25 April 2022)

We propose doubly ionized lanthanum ( $\text{La}^{2+}$ ) as a possible qubit candidate for quantum networks. Transitions between the lowest levels in the atom are in the infrared, enabling a direct matter-light interface amenable to long-distance quantum communication. These transitions could also be used to directly laser-cool trapped  $\text{La}^{2+}$  ions. The rich hyperfine structure of the ion may allow for a qubit stored in magnetic-field insensitive states as well as protocols for atom-photon entanglement.

DOI: [10.1103/PhysRevA.105.042617](https://doi.org/10.1103/PhysRevA.105.042617)

### I. INTRODUCTION

Quantum information has the potential to revolutionize computation and communication. Trapped atomic ions are a leading platform for applications in quantum information, due in part to their long coherence times [1–4], and precise control and detection of the atomic quantum states using microwave and laser radiation [2,5–7]. These pristine quantum systems continue to extend the frontiers of quantum computation [8–12], quantum simulation [13–15], and quantum sensing [16,17].

Trapped atomic ions are also a candidate for quantum networks [18–23]. Pioneering experiments have demonstrated the ability to entangle ions remotely, over considerable distance, using their emitted photons [24–27]. In general, however, the ultraviolet and visible wavelengths of photons directly produced by strong transitions between low-lying levels in atomic ions [9] are not conducive to long-distance transmission through optical fibers [28,29]. Nevertheless, recent experiments demonstrated the ability to convert the short-wavelength photons emitted by trapped ions to the infrared frequencies more amenable to long-distance communication [30–39]. These experiments represent a promising approach to quantum networks with trapped ions, even though the frequency-conversion stage adds noise and loss as well as additional complexity to an already intricate system.

Here, doubly ionized lanthanum ( $\text{La}^{2+}$ ) is proposed as an alternative approach to quantum networks. Transitions between the lowest-lying levels in  $\text{La}^{2+}$  are in the infrared with low-loss transmission in standard optical fiber and may be used for laser cooling. The rich hyperfine structure of the ion allows for magnetic-field insensitive qubit states as well as state detection fidelities comparable to other atomic ions and methods for directly producing ion-photon entanglement at wavelengths amenable to long-distance transmission for the realization of quantum networks.

### II. ATOMIC STRUCTURE AND LASER COOLING

The lowest levels in doubly ionized lanthanum are  $^2D_{3/2}$  and  $^2D_{5/2}$ , followed by  $^2F_{5/2}^o$  and  $^2F_{7/2}^o$ , as shown in Fig. 1. The  $^2F_{5/2}^o$  and  $^2F_{7/2}^o$  levels are predicted to have lifetimes of about 4.6 and 4.4  $\mu\text{s}$ , respectively, whereas the metastable  $^2D_{5/2}$  is predicted to have a lifetime of about 15 s [40]. All four low-lying levels have substantial hyperfine structure as both naturally occurring isotopes have relatively large nuclear spin: the  $^{139}\text{La}$  isotope has a natural abundance of 99.91% and nuclear spin  $I = 7/2$ ; the  $^{138}\text{La}$  isotope has a natural abundance of 0.09% and nuclear spin  $I = 5$  [41]. The large nuclear spin combined with the substantial  $J$  values of the electronic levels results in a rich hyperfine structure that has recently been measured [42] and calculated [43] for the  $^{139}\text{La}$  isotope. Despite multiple hyperfine manifolds, the ion is tractable for laser cooling.

Trapped  $\text{La}^{2+}$  ions could be laser cooled by using either a three-level ( $\Lambda$ -type) or four-level scheme. A possible three-level cooling scheme involves driving the  $^2D_{3/2} \leftrightarrow ^2F_{5/2}^o$  transition near 1389.4 nm (air) along with the  $^2D_{3/2} \leftrightarrow ^2F_{5/2}^o$  transition near 1787.8 nm (air) as shown in Fig. 1(a). This three-level cooling scheme would be similar to the approach often used for cooling other trapped ions with a low-lying  $D$  level, including  $\text{Ca}^+$  [45],  $\text{Sr}^+$  [46], and  $\text{Ba}^+$  [47], and is susceptible to coherent population trapping [48]. Alternatively, a possible four-level cooling scheme involves driving the  $^2D_{3/2} \leftrightarrow ^2F_{5/2}^o$  transition near 1389.4 nm (air) and the  $^2D_{5/2} \leftrightarrow ^2F_{7/2}^o$  transition near 1409.6 nm (air) as shown in Fig. 1(b), which would be similar to the approach often used for cooling  $\text{Yb}^+$  [49,50]. In either case, all necessary frequencies for laser cooling can be generated by just two lasers with wavelengths accessible using semiconductor diode lasers.

The four-level cooling scheme has potential advantages. First, this option has the important technical advantage that the two required laser wavelengths are near enough to each other that a common set of fibers and optics may be used. Second, in this case there exists a true cycling transition between the  $^2D_{5/2}$  ( $|F = 6\rangle$ ) and the  $^2F_{7/2}^o$  ( $|F = 7\rangle$ ) levels, despite the substantial hyperfine structure of  $^{139}\text{La}^{2+}$ . Population accumulated in other hyperfine levels, through

\*steven.olmschenk@denison.edu

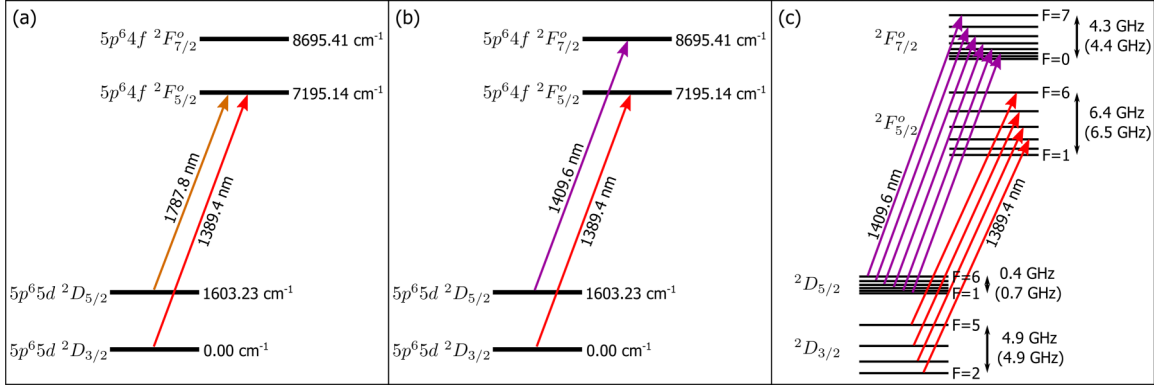


FIG. 1. Energy-level diagram of  $\text{La}^{2+}$  with possible laser-cooling schemes. (a) A three-level cooling scheme driving the  ${}^2D_{3/2} \leftrightarrow {}^2F_{5/2}^o$  transition near 1389.4 nm and the  ${}^2D_{3/2} \leftrightarrow {}^2F_{7/2}^o$  transition near 1787.8 nm. (b) A four-level cooling scheme driving the  ${}^2D_{3/2} \leftrightarrow {}^2F_{5/2}^o$  transition near 1389.4 nm and the  ${}^2D_{5/2} \leftrightarrow {}^2F_{7/2}^o$  transition near 1409.6 nm. (c) The four-level cooling scheme with hyperfine structure shown (not to scale) with light driving each  ${}^2D |F = n\rangle$  to  ${}^2F^o |F = n + 1\rangle$  transition. Here each top (bottom, parenthetical) frequency gives the extent of the hyperfine manifold splitting calculated from the experimental (theoretical) hyperfine  $A$  and  $B$  coefficients given in Ref. [42] (Ref. [43]). Wavelengths given in air [44].

off-resonant scattering and other processes, can be optically pumped to this cycling transition by driving each  ${}^2D |F = n\rangle$  to  ${}^2F^o |F = n + 1\rangle$  transition as illustrated in Fig. 1(c). The additional required frequencies may be produced by wide-bandwidth fiber electro-optic modulators (standard components at these wavelengths) driven at multiple frequencies to generate sidebands on the laser light for depopulating all hyperfine levels in  ${}^2D_{3/2}$  and  ${}^2D_{5/2}$ . Therefore, two lasers and two fiber electro-optic modulators can produce all required frequencies for laser cooling.

The aforementioned lifetime of the  ${}^2F_{5/2}^o$  and  ${}^2F_{7/2}^o$  levels [40] results in a Doppler-cooling temperature limit of less than  $1 \mu\text{K}$ , which might make  $\text{La}^{2+}$  ions attractive for setups involving sympathetic cooling. On the other hand, these relatively long lifetimes also limit the photon scattering rate from  $\text{La}^{2+}$  ions, which is important for fluorescence detection of trapped ions and state detection of a potential  $\text{La}^{2+}$  hyperfine qubit.

### III. HYPERFINE QUBIT

Qubits stored in the hyperfine levels of a trapped ion can exhibit simple state preparation, long coherence times and high-fidelity state detection (for a review of different qubit realizations in trapped atomic ions, see, e.g., Refs. [9,51]). We consider a hyperfine qubit in  ${}^{139}\text{La}^{2+}$  stored in states in the  ${}^2D_{5/2} |F = 5\rangle$  and  $|F = 6\rangle$  hyperfine manifolds.

Initialization of a qubit into a defined pure state is the first step in most quantum information protocols. Doubly ionized lanthanum could be prepared in the  ${}^2D_{5/2} |F = 6, m_F = +6\rangle$  or  $|F = 6, m_F = -6\rangle$  state by optical pumping with  $\sigma^+$ - or  $\sigma^-$ -polarized light, respectively. Optical pumping with  $\sigma^-$ -polarized light to  $|F = 6, m_F = -6\rangle$  may be preferred to red-detune the incident laser light from all  ${}^2D_{5/2} |F = 5, 6\rangle \leftrightarrow {}^2F_{7/2}^o |F = 6, 7\rangle$  transitions while optimizing the scattering rate on the cycling transition. Although state preparation fidelity based on optical pumping in hyperfine qubits with nuclear spin greater than  $1/2$  is typically limited by the polarization purity of the laser light, it can be improved

by combining optical pumping with additional optical or microwave transitions [2,5,52]. A subsequent series of microwave transitions could then move population to any state in the hyperfine manifold, including pairs of states that are first-order insensitive to magnetic-field fluctuations.

Qubits that are first-order insensitive to magnetic fields are important for achieving long coherence times. We calculated the energy shift of states in the low-lying levels of  ${}^{139}\text{La}^{2+}$  by numerically diagonalizing the Hamiltonian for the hyperfine interaction in the presence of an external magnetic field [53],

$$H_{\text{hfs}} = A_{\text{hfs}} \mathbf{I} \cdot \mathbf{J} + B_{\text{hfs}} \frac{6(\mathbf{I} \cdot \mathbf{J})^2 + 3(\mathbf{I} \cdot \mathbf{J}) - 2I(I+1)J(J+1)}{2I(2I-1)2J(2J-1)} + g_J \mu_B B J_z + g_I \mu_B B I_z,$$

where  $A_{\text{hfs}}$  is the magnetic dipole hyperfine coefficient,  $B_{\text{hfs}}$  is the electric quadrupole hyperfine coefficient,  $I$  is the nuclear spin and  $I_z$  is its projection along the magnetic field,  $J$  is the total electron spin and  $J_z$  is its projection along the magnetic field,  $\mu_B$  is the Bohr magneton,  $B$  is the magnetic field defined to be in the  $z$  direction,  $g_J$  is the Landé  $g$  factor, and  $g_I$  is the nuclear  $g$  factor using the convention of Ref. [53]. We repeated the calculation for both the experimentally [42] and the theoretically [43] determined values for the hyperfine coefficients and searched for pairs of states in the  ${}^2D_{5/2} |F = 5\rangle$  and  $|F = 6\rangle$  hyperfine manifolds where the first-order derivative of the frequency difference vanishes at finite magnetic field (see Fig. 2). Several options for a first-order magnetic-field-insensitive qubit are listed in Table I.

A qubit stored in  ${}^2D_{5/2} |F = 5, m_F = 1\rangle$  and  $|F = 6, m_F = 1\rangle$ , calculated to be first-order magnetic-field insensitive at an external field of about 0.18 (0.64) mT using the experimentally (theoretically) determined hyperfine coefficients, is of particular interest. In this case, the small external magnetic field required is easily obtained in the laboratory. Additionally, at this magnetic field the induced shift in transition frequencies from  ${}^2D_{5/2} |F = 6\rangle$  to  ${}^2F_{7/2}^o |F = 7\rangle$  for the  $\sigma^-$ -polarized light span about 2 (8) MHz across all states,

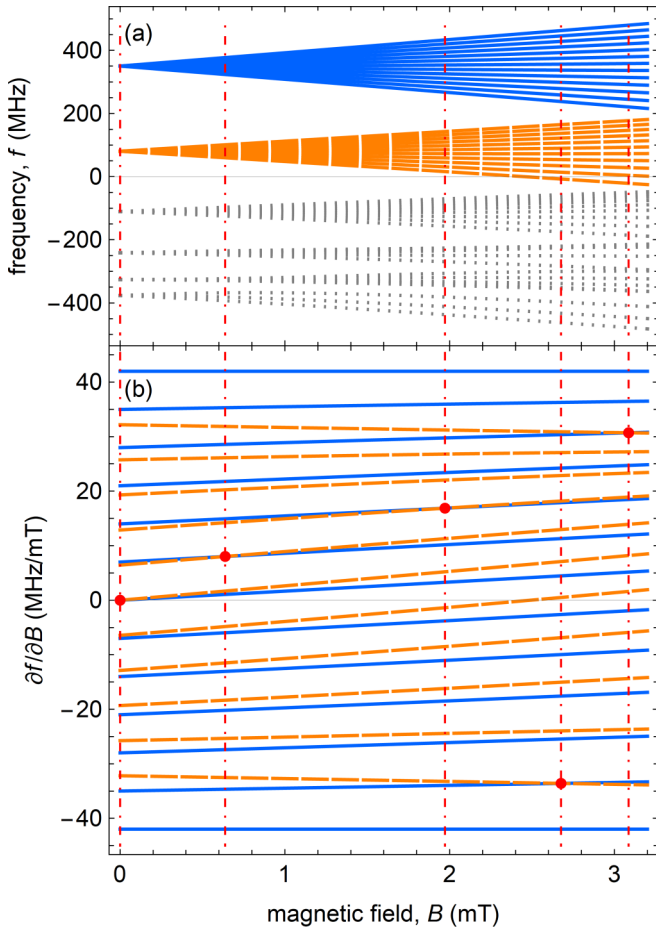


FIG. 2. Calculating the hyperfine interaction in the presence of an external magnetic field is used to identify possible qubit states with splitting first-order insensitive to the magnetic field. (a) Frequency shift ( $f$ ) of states in  ${}^2D_{5/2}$  as a function of magnetic-field ( $B$ ) using the theoretical hyperfine coefficients from Ref. [43]. (b) First-order derivative of the  $F = 5, 6$  frequency shifts in (a) with respect to the magnetic-field ( $\partial f/\partial B$ ). Solid blue lines are states in the  $F = 6$  manifold, dashed orange lines are states in the  $F = 5$  manifold, red points are where two states have identical derivatives and indicate possible first-order magnetic-field insensitive qubits (see Table I), and vertical red dot-dashed lines highlight the strength of the external magnetic field at these points.

making the manifold addressable by a single laser frequency of reasonable ( $\sim 1$  MHz) linewidth. As noted in Table I, the splitting between this pair of states is calculated to have a second-order magnetic-field dependence of about  $1.5 \text{ Hz}/\mu\text{T}^2$  ( $0.43 \text{ Hz}/\mu\text{T}^2$ ), comparable to the sensitivity of other qubits with demonstrated long coherence times [1].

The qubit state could be readout using standard state-dependent fluorescence [9,51,54] with  ${}^2D_{5/2} |F = 6, m_F = 1\rangle$  as the resonant “bright” state and  ${}^2D_{5/2} |F = 5, m_F = 1\rangle$  as the off-resonant “dark” state as illustrated in Fig 3. Modeling the system similar to Refs. [55,56], we find that errors in state detection due to off-resonant coupling to other states should be small due to the relatively large detuning with respect to linewidth for both the bright and the dark states. Even when considering the expected linewidth of the detection laser (1 MHz), the detuning to unintended states is

TABLE I. Partial list of options for qubits in the  ${}^2D_{5/2} |F = 6\rangle$  and  $|F = 5\rangle$  hyperfine manifolds with energy splittings that are first-order insensitive to magnetic fields at relatively small fields. The first column gives the pair of states comprising the qubit where states are denoted as  $|F, m_F\rangle$ . The second column is the value of the magnetic field (in millitesla) where first-order dependence vanishes. The third column is the remaining second-order sensitivity to the magnetic field (in  $\text{Hz}/\mu\text{T}^2$ ). In both the second and third columns, the first value is calculated using the experimentally determined hyperfine coefficients from Ref. [42] with an estimated uncertainty determined by propagating the experimental uncertainties in the hyperfine coefficients, and the second (parenthetical) value is calculated using the theoretical hyperfine coefficients from Ref. [43].

Qubit states	Magnetic field (mT)	Sensitivity ( $\text{Hz}/\mu\text{T}^2$ )
$ 5, 0\rangle \leftrightarrow  6, 0\rangle$	0	$1.7 \pm 0.8$ (0.49)
$ 5, 1\rangle \leftrightarrow  6, 1\rangle$	$0.18 \pm 0.07$ (0.64)	$1.5 \pm 0.8$ (0.43)
$ 5, 2\rangle \leftrightarrow  6, 2\rangle$	$0.4 \pm 0.2$ (2.0)	$1.2 \pm 0.7$ (0.23)
$ 5, -5\rangle \leftrightarrow  6, -5\rangle$	$2.0 \pm 0.4$ (2.7)	$0.7 \pm 0.2$ (0.53)
$ 5, 5\rangle \leftrightarrow  6, 4\rangle$	$2.3 \pm 0.4$ (3.1)	$0.9 \pm 0.2$ (0.64)

approximately  $10^3$  linewidths, which is larger than the detuning in several other ions with demonstrated high-fidelity state detection of hyperfine qubits (e.g.,  ${}^{111}\text{Cd}^+$  with off-resonant coupling from the dark state detuned by about  $2 \times 10^2$  linewidths [55];  ${}^{171}\text{Yb}^+$  with off-resonant coupling from the bright state detuned by about  $10^2$  linewidths [50,57]). Leakage out of the bright and dark state manifolds is further suppressed by small electric dipole transition probabilities between the off-resonantly coupled states, relative to the cycling transition. Error in bright state detection is also suppressed

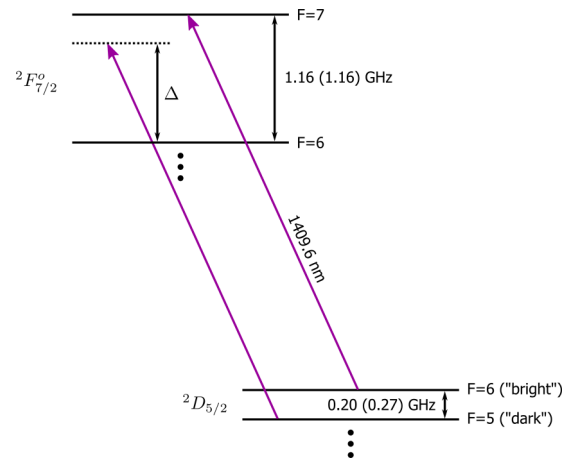


FIG. 3. Qubit state readout using standard state-dependent fluorescence. Near-resonant,  $\sigma^-$ -polarized, laser light drives the  ${}^2D_{5/2} |F = 6\rangle$  to  ${}^2F_{7/2} |F = 7\rangle$  transition, driving population in the  ${}^2D_{5/2} |F = 6, m_F = 1\rangle$  qubit state to the cycling transition, scattering many photons and appearing bright to a detector. This laser light is detuned from the nearest transition involving the  ${}^2D_{5/2} |F = 5, m_F = 1\rangle$  qubit state by  $\Delta = 0.96$  (0.89) GHz, the difference between the  ${}^2F_{7/2} F = 6 \leftrightarrow 7$  and the  ${}^2D_{5/2} F = 5 \leftrightarrow 6$  hyperfine splittings and, therefore, appears dark to a detector. Hyperfine splittings are calculated from the experimental (theoretical) hyperfine  $A$  and  $B$  coefficients given in Ref. [42] (Ref. [43]). The energy-level diagram is partial and not to scale. Wavelength given in air [44].

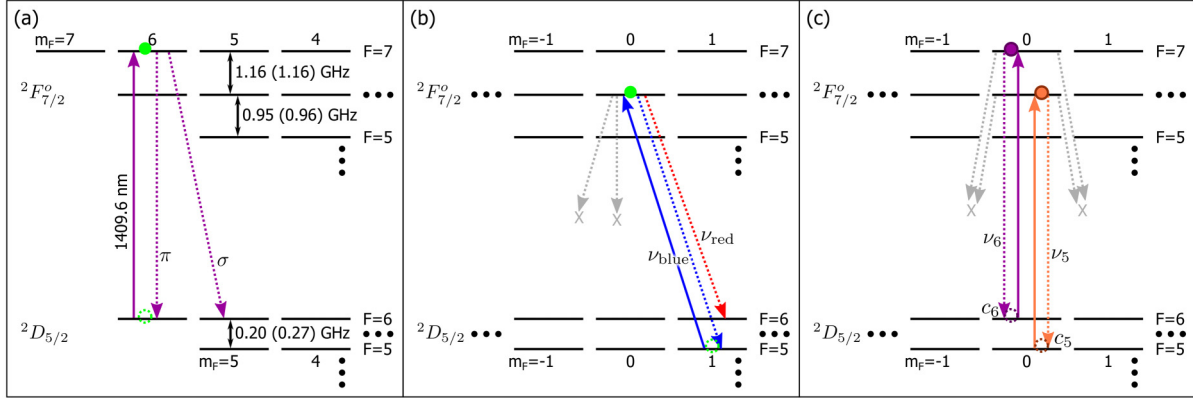


FIG. 4. Ion-photon entanglement protocols discussed in the text where dotted circles represent the initially prepared atomic state(s), filled circles represent the state(s) excited by the laser pulse, solid lines represent the transition(s) driven by the laser pulse, dotted lines represent decay (photon emission) transitions, and the hyperfine splittings are calculated from the experimental (theoretical) hyperfine  $A$  and  $B$  coefficients given in Ref. [42] (Ref. [43]). Energy-level diagrams are partial and not to scale. Wavelength given in air [44]. (a) Polarization-encoded photonic qubit: The polarization of the photon (here  $\pi$  and  $\sigma$ ) is entangled with the final atomic state. Collecting photons in a direction perpendicular to a quantization axis defined by an external magnetic field,  $\pi$  and  $\sigma$  polarizations are linearly polarized and orthogonal. (b) Frequency-encoded photonic qubit: The (resolved) frequency of the emitted photon (here  $\nu_{\text{red}}$  and  $\nu_{\text{blue}}$ ) is entangled with the final atomic state. Collecting photons along a quantization axis defined by an external magnetic field allows filtering-out  $\pi$ -polarized light (vertical, gray, dotted line with X) based on the dipole radiation pattern, and  $\sigma^+$ -polarized light (diagonal, gray, dotted line with X) using a quarter-wave plate and polarizer. (c) Amplitude-preserving frequency-encoded photonic qubit: The (resolved) frequency of the emitted photon (here  $\nu_5$  and  $\nu_6$ ) is entangled with the final atomic state. Collecting photons in a direction perpendicular to a quantization axis defined by an external magnetic field,  $\pi$  and  $\sigma$  polarizations are linearly polarized and orthogonal, allowing  $\sigma$ -polarized light (diagonal, gray, dotted lines with X) to be filtered out. Conditioned on this filtering, and due to selection rules, the initially prepared atomic amplitudes  $c_5$  and  $c_6$  may be preserved.

due to the dependence on polarization errors; either  $\pi$ - or  $\sigma^+$ -polarized light is required to couple  ${}^2D_{5/2} |F=6, m_F=-6\rangle$  to off-resonant states instead of driving the cycling transition. However, decay of the  ${}^2D_{5/2}$  level appears as an additional error in bright state detection. Another important consideration in our model is the error contribution from background counts, given the small photon scattering rate resulting from the relatively long lifetime of the  ${}^2F_{7/2}$  level. Nevertheless, given the high detection efficiency and low dark count rate of available superconducting nanowire single-photon detectors (SNSPDs), high state detection fidelities may still be achieved. Altogether, assuming a simple threshold detection method, modest light collection optics (numerical aperture = 0.28), a wide range of laser intensities ( $\lesssim 15 \times$  saturation intensity), and detection parameters readily achieved with an SNSPD (quantum efficiency  $\approx 0.8$ , dark count rate  $\leq 2 \text{ s}^{-1}$ , fiber coupling  $\approx 0.2$ ), our model already predicts a state detection fidelity greater than 99.9%. The fidelity increases by considering larger light collection [38,50,55,57–66], larger fiber coupling [27], or a smaller laser linewidth (e.g., comparable to the natural linewidth of the transition).

The potential for first-order magnetic-field-insensitive qubit states with high-fidelity state preparation and readout supports  ${}^{139}\text{La}^{2+}$  as an excellent quantum memory candidate, comparable to current trapped ion qubits with possible applications in photon-mediated entanglement operations.

#### IV. PHOTONIC ENTANGLEMENT

Entanglement between an atomic ion and an emitted photon can serve as the foundation for a quantum network

where linking ions over a long distance is accomplished by the interference and detection of spontaneously emitted photons [18–23]. Doubly ionized lanthanum is an excellent candidate for this architecture as it could be entangled with the polarization or frequency mode of a photon with emitted wavelengths directly amenable to long-distance transmission.

A possible protocol for entangling  ${}^{139}\text{La}^{2+}$  with the polarization of an emitted photon is illustrated in Fig. 4(a). The ion would be initially prepared in the  ${}^2D_{5/2} |F=6, m_F=-6\rangle$  state by optical pumping with  $\sigma^-$ -polarized light. A 10-ns  $\pi$ -polarized laser pulse then could excite the atom to the  ${}^2F_{7/2} |F=7, m_F=-6\rangle$  state. Notably, an excitation pulse of 10 ns would be much shorter than the lifetime of the excited state (inhibiting multiple excitation-emission processes), yet result in a pulse linewidth significantly smaller than the excited-state hyperfine splitting (inhibiting off-resonant coupling to other states). We estimate the optimal pulse duration is about 10 ns (although this value will depend on the time-bandwidth product of the pulse) with estimated errors due to double excitation and off-resonant scattering each less than  $3 \times 10^{-3}$ . Following excitation, the subsequent atomic decay and photon emission ideally produces the ion-photon entangled state  $|\Psi\rangle = \sqrt{\frac{1}{7}}|6, -6\rangle|\pi\rangle + \sqrt{\frac{6}{7}}|6, -5\rangle|\sigma\rangle$  where the atomic state is denoted by the final  $F$  and  $m_F$  values in the  ${}^2D_{5/2}$  level, the photonic state is denoted by the polarization  $\pi$  or  $\sigma$ , and the coefficients arise from the dipole transition matrix element for each decay channel. Collecting emitted photons in a direction perpendicular to a quantization axis defined by an external magnetic field, where  $\pi$  and  $\sigma$

polarizations are linearly polarized and orthogonal, and the intensity of radiation of the  $\pi$  decay is twice as strong as the  $\sigma$  decay, would result in an ion-photon entangled state  $|\Psi\rangle = \frac{1}{2}|6, -6\rangle|V\rangle + \frac{\sqrt{3}}{2}|6, -5\rangle|H\rangle$  where we now denote the two (linear and orthogonal) polarizations as  $V$  and  $H$  [67,68]. This protocol has the advantage of simple state preparation and straightforward manipulation of the photonic state using wave plates and polarizers, although it does not directly connect to a magnetic-field-insensitive pair of states for the ion.

One option for entangling a first-order magnetic-field-insensitive atomic qubit with the frequency of an emitted photon is shown in Fig. 4(b). In this case, following optical pumping to  ${}^2D_{5/2} |F = 6, m_F = -6\rangle$ , a series of microwave transitions could move the population to  ${}^2D_{5/2} |F = 5, m_F = 1\rangle$ . A 10-ns  $\sigma^-$ -polarized laser pulse then could excite the atom to the  ${}^2F_{7/2}^o |F = 6, m_F = 0\rangle$  state with estimated errors due to double excitation and off-resonant scattering nearly the same as the polarization-encoded protocol. Collecting photons in a direction along a quantization axis defined by an external magnetic field, the dipole radiation pattern of  $\pi$ -polarized light does not couple into a single-mode optical fiber, and  $\sigma^+$  and  $\sigma^-$  transitions produce light with orthogonal circular polarizations that may be converted to orthogonal linear polarizations using quarter-wave plates [61,68–70]. The atomic decay and photon emission, combined with appropriate filtering to select only the  $\sigma^-$ -polarized photons, then ideally produces the ion-photon entangled state  $|\Psi\rangle = \sqrt{\frac{25}{36}}|5, 1\rangle|v_{\text{blue}}\rangle + \sqrt{\frac{11}{36}}|6, 1\rangle|v_{\text{red}}\rangle$  where the atomic state is again denoted by the final  $F$  and  $m_F$  values in the  ${}^2D_{5/2}$  level and the photonic state is denoted by the frequency  $v_{\text{blue}}$  or  $v_{\text{red}}$ , which approximately differ by the hyperfine splitting of  $F = 5$  and  $F = 6$  in  ${}^2D_{5/2}$  [ $v_{\text{blue}} - v_{\text{red}} = 0.20$  (0.27) GHz] and are well resolved due to the narrow linewidth of the transition ( $\gamma = 2\pi \times 36$  kHz). These resulting atomic states can be first-order magnetic-field insensitive (see Table I), and the frequency-encoded photonic states should be resilient against dispersion and birefringence [68,71,72].

An alternative frequency-encoded photonic qubit protocol is presented in Fig. 4(c) where the ion is prepared in a superposition of  ${}^2D_{5/2} |F = 5, m_F = 0\rangle$  and  $|F = 6, m_F = 0\rangle$ , then excited to  ${}^2F_{7/2}^o$  using  $\pi$ -polarized light. Driving the ion with two frequencies, and noting the elimination of nearest-state off-resonant coupling due to selection rules, a few-nanosecond laser pulse could simultaneously drive the  ${}^2D_{5/2} |F = 5, m_F = 0\rangle$  to  ${}^2F_{7/2}^o |F = 6, m_F = 0\rangle$  and  ${}^2D_{5/2} |F = 6, m_F = 0\rangle$  to  ${}^2F_{7/2}^o |F = 7, m_F = 0\rangle$  transitions with estimated errors due to double excitation and off-resonant scattering each less than  $1 \times 10^{-3}$ . Collecting photons in a direction perpendicular to a quantization axis defined by an external magnetic field allows for polarization filtering to select only photons from  $\pi$  transitions. Then due to selection rules, the resulting ion-photon entangled state is ideally  $|\Psi\rangle = a_5 c_5 |5, 0\rangle|v_5\rangle + a_6 c_6 |6, 0\rangle|v_6\rangle$  where the atomic state is again denoted by the final  $F$  and  $m_F$  values in the  ${}^2D_{5/2}$  level, the photonic state is denoted by the resolved frequency  $v_5$  or  $v_6$  such that  $v_6 - v_5 = 0.96$  (0.89) GHz (the difference between the  ${}^2F_{7/2}^o$   $F = 6 \leftrightarrow 7$  and the  ${}^2D_{5/2}$   $F = 5 \leftrightarrow 6$  hyperfine splittings), the initial amplitudes of  ${}^2D_{5/2} |F =$

$5, m_F = 0\rangle$  and  $|F = 6, m_F = 0\rangle$  are denoted by  $c_5$  and  $c_6$ , and the effect of the excitation laser pulse and dipole transition matrix element are incorporated into  $a_5$  and  $a_6$ . Notably, it should be possible to tailor the excitation laser pulse properties such that  $a_5$  and  $a_6$  can be assigned arbitrary relative values, including  $a_5 = a_6 = 1$ . In that case, the ion-photon entangled state becomes  $|\Psi\rangle = c_5 |5, 0\rangle|v_5\rangle + c_6 |6, 0\rangle|v_6\rangle$  and may facilitate a photon-mediated quantum gate between remote atoms [25,71,73].

Additional ion-photon entanglement protocols can be devised to connect to other potential atomic qubit states in Table I (and more beyond these). Moreover, other photonic qubits can be considered, such as using two successive excitations of the cycling transition to produce a time-bin encoded photonic qubit [69,74–76]. In all cases, photons at this wavelength are expected to experience  $\leq 0.32$  dB/km attenuation in standard optical fiber [77,78].

Although photonic entanglement protocols can be mostly insensitive to the motional state of the ion [22,68,71], motional modes may be an important consideration for quantum network architectures that use both photonic entanglement and deterministic motional gates [21,22,79,80]. One source of error in motional gates is motional heating in radio-frequency (rf) ion traps where the motional heating rate is  $\dot{n} = [q^2 / (4m\hbar\omega)] S_E(\omega)$  with  $q$  as the ion electric charge,  $m$  as the ion mass,  $\omega$  as the motional frequency of the trapped ion, and  $S_E(\omega)$  as the electric-field noise spectral density [81,82]. Recent experiments indicate frequency scaling of  $S_E(\omega) \propto 1/\omega^\alpha$  with  $\alpha$  between about 1 to 1.5 [11]. Since the transverse secular frequency in a linear rf trap is  $\omega_r \propto q$  [54], then for a given trap voltage and geometry, transverse motional heating should be approximately independent of  $q$ ; in the axial direction  $\omega_z \propto \sqrt{q}$  [54], which results in axial motional heating that scales as  $q^\beta$  with  $\beta \lesssim 1$ . Larger motional frequencies can also allow for faster motional gates [9,83] and, thereby, reduce the impact of motional heating. Altogether, the electric charge of doubly ionized lanthanum is not expected to limit its applicability in architectures that require motional coupling.

The rate of ion-photon entanglement is an also important consideration for large-scale quantum networks. Although the per atom repetition rate for producing ion-photon entanglement is bounded by the relatively long lifetime of the  ${}^2F_{7/2}^o$  excited state in  ${}^{139}\text{La}^{2+}$  ( $\tau = 4.4 \mu\text{s}$  [40];  $\gamma = 2\pi \times 36$  kHz), for distances greater than about 5 km between network nodes, the limitation to the per atom repetition rate will be the propagation delay for the photon and (classical) detection signal [84,85]. As with any trapped ion system facing this distance-limited rate, the probability of successfully registering entanglement over long distances can be improved by incorporating high numerical aperture optics [57,59–62] or an optical cavity [38,63–66] for efficient photon collection, and the effective rate can be increased by multiplexing a system with multiple communication ions [38,79,80,86,87]. Therefore, doubly ionized lanthanum should be able to provide ion-photon entanglement rates over long distances comparable to other ions and may have a distinct advantage by directly producing the telecom-compatible photons amenable to transmission over these distances.

## V. CONCLUSION

Doubly ionized lanthanum may allow for efficient laser cooling using infrared diode lasers, a range of first-order magnetic-field-insensitive qubit states with high-fidelity state detection, and viable protocols for directly entangling trapped ions with telecom-compatible photons for long-distance transmission in optical fiber. The unique features of doubly ionized lanthanum may also make it a candidate for other quantum information applications, including as a refrigerant ion [88–91] (given the small Doppler-cooling temperature limit and large difference in wavelength compared to other trapped ions) or a multistate qudit candidate [92–96] (given the rich hyperfine

structure). While the results presented here are promising, more precise measurements of the hyperfine structure of doubly ionized lanthanum, as well as additional investigations into producing and trapping multiply charged ions, may be needed to realize the potential of doubly ionized lanthanum for applications in quantum information and quantum networks.

## ACKNOWLEDGMENTS

This material is based upon work supported by the National Science Foundation under Grant No. 1752685.

- 
- [1] C. Langer, R. Ozeri, J. D. Jost, J. Chiaverini, B. DeMarco, A. Ben-Kish, R. B. Blakestad, J. Britton, D. B. Hume, W. M. Itano, D. Leibfried, R. Reichle, T. Rosenband, T. Schaetz, P. O. Schmidt, and D. J. Wineland, Long-Lived Qubit Memory Using Atomic Ions, *Phys. Rev. Lett.* **95**, 060502 (2005).
- [2] T. P. Harty, D. T. C. Allcock, C. J. Ballance, L. Guidoni, H. A. Janacek, N. M. Linke, D. N. Stacey, and D. M. Lucas, High-Fidelity Preparation, Gates, Memory, and Readout of a Trapped-Ion Quantum Bit, *Phys. Rev. Lett.* **113**, 220501 (2014).
- [3] Y. Wang, M. Um, J. Zhang, S. An, M. Lyu, J.-N. Zhang, L.-M. Duan, D. Yum, and K. Kim, Single-qubit quantum memory exceeding ten-minute coherence time, *Nat. Photonics* **11**, 646 (2017).
- [4] P. Wang, C.-Y. Luan, M. Qiao, M. Um, J. Zhang, Y. Wang, X. Yuan, M. Gu, J. Zhang, and K. Kim, Single ion qubit with estimated coherence time exceeding one hour, *Nat. Commun.* **12**, 233 (2021).
- [5] J. P. Gaebler, T. R. Tan, Y. Lin, Y. Wan, R. Bowler, A. C. Keith, S. Glancy, K. Coakley, E. Knill, D. Leibfried, and D. J. Wineland, High-fidelity universal gate set for  $^9\text{Be}^+$  ion qubits, *Phys. Rev. Lett.* **117**, 060505 (2016).
- [6] J. E. Christensen, D. Hucul, W. C. Campbell, and E. R. Hudson, High-fidelity manipulation of a qubit enabled by a manufactured nucleus, *npj Quantum Inf.* **6**, 35 (2020).
- [7] L. A. Zhukas, P. Svihra, A. Nomerotski, and B. B. Blinov, High-fidelity simultaneous detection of a trapped-ion qubit register, *Phys. Rev. A* **103**, 062614 (2021).
- [8] R. Blatt and D. J. Wineland, Entangled states of trapped atomic ions, *Nature (London)* **453**, 1008 (2008).
- [9] C. D. Bruzewicz, J. Chiaverini, R. McConnell, and J. M. Sage, Trapped-ion quantum computing: Progress and challenges, *Appl. Phys. Rev.* **6**, 021314 (2019).
- [10] Y. Alexeev, D. Bacon, K. R. Brown, R. Calderbank, L. D. Carr, F. T. Chong, B. DeMarco, D. Englund, E. Farhi, B. Fefferman, A. V. Gorshkov, A. Houck, J. Kim, S. Kimmel, M. Lange, S. Lloyd, M. D. Lukin, D. Maslov, P. Maunz, C. Monroe *et al.*, Quantum computer systems for scientific discovery, *PRX Quantum* **2**, 017001 (2021).
- [11] K. R. Brown, J. Chiaverini, J. M. Sage, and H. Häffner, Materials challenges for trapped-ion quantum computers, *Nat. Rev. Mater.* **6**, 892 (2021).
- [12] N. P. de Leon, K. M. Itoh, D. Kim, K. K. Mehta, T. E. Northup, H. Paik, B. S. Palmer, N. Samarth, S. Sangtawesin, and D. W. Steuerman, Materials challenges and opportunities for quantum computing hardware, *Science* **372**, eabb2823 (2021).
- [13] R. Blatt and C. F. Roos, Quantum simulations with trapped ions, *Nat. Phys.* **8**, 277 (2012).
- [14] C. Monroe, W. C. Campbell, L.-M. Duan, Z.-X. Gong, A. V. Gorshkov, P. Hess, R. Islam, K. Kim, N. Linke, G. Pagano, P. Richerme, C. Senko, and N. Y. Yao, Programmable quantum simulations of spin systems with trapped ions, *Rev. Mod. Phys.* **93**, 025001 (2021).
- [15] E. Altman, K. R. Brown, G. Carleo, L. D. Carr, E. Demler, C. Chin, B. DeMarco, S. E. Economou, M. A. Eriksson, K.-M. C. Fu, M. Greiner, K. R. A. Hazzard, R. G. Hulet, A. J. Kollár, B. L. Lev, M. D. Lukin, R. Ma, X. Mi, S. Misra, C. Monroe *et al.*, Quantum simulators: Architectures and opportunities, *PRX Quantum* **2**, 017003 (2021).
- [16] A. D. Ludlow, M. M. Boyd, J. Ye, E. Peik, and P. O. Schmidt, Optical atomic clocks, *Rev. Mod. Phys.* **87**, 637 (2015).
- [17] C. L. Degen, F. Reinhard, and P. Cappellaro, Quantum sensing, *Rev. Mod. Phys.* **89**, 035002 (2017).
- [18] H.-J. Briegel, W. Dür, J. I. Cirac, and P. Zoller, Quantum Repeaters: The Role of Imperfect Local Operations in Quantum Communication, *Phys. Rev. Lett.* **81**, 5932 (1998).
- [19] C. Simon and W. T. M. Irvine, Robust Long-Distance Entanglement and a Loophole-Free Bell Test with Ions and Photons, *Phys. Rev. Lett.* **91**, 110405 (2003).
- [20] H. J. Kimble, The quantum internet, *Nature (London)* **453**, 1023 (2008).
- [21] N. Sangouard, R. Dubessy, and C. Simon, Quantum repeaters based on single trapped ions, *Phys. Rev. A* **79**, 042340 (2009).
- [22] L.-M. Duan and C. Monroe, Colloquium: Quantum networks with trapped ions, *Rev. Mod. Phys.* **82**, 1209 (2010).
- [23] D. Awschalom, K. K. Berggren, H. Bernien, S. Bhave, L. D. Carr, P. Davids, S. E. Economou, D. Englund, A. Faraon, M. Fejer, S. Guha, M. V. Gustafsson, E. Hu, L. Jiang, J. Kim, B. Kozh, P. Kumar, P. G. Kwiat, M. Lončar, M. D. Lukin *et al.*, Development of quantum interconnects (QuICs) for next-generation information technologies, *PRX Quantum* **2**, 017002 (2021).
- [24] D. L. Moehring, P. Maunz, S. Olmschenk, K. C. Younge, D. N. Matsukevich, L.-M. Duan, and C. Monroe, Entanglement of single-atom quantum bits at a distance, *Nature (London)* **449**, 68 (2007).
- [25] S. Olmschenk, D. N. Matsukevich, P. Maunz, D. Hayes, L.-M. Duan, and C. Monroe, Quantum teleportation between distant matter qubits, *Science* **323**, 486 (2009).
- [26] D. Hucul, I. V. Inlek, G. Vittorini, C. Crocker, S. Debnath, S. M. Clark, and C. Monroe, Modular entanglement of

- atomic qubits using photons and phonons, *Nat. Phys.* **11**, 37 (2015).
- [27] L. J. Stephenson, D. P. Nadlinger, B. C. Nichol, S. An, P. Drmota, T. G. Ballance, K. Thirumalai, J. F. Goodwin, D. M. Lucas, and C. J. Ballance, High-Rate, High-Fidelity Entanglement of Qubits Across an Elementary Quantum Network, *Phys. Rev. Lett.* **124**, 110501 (2020).
- [28] P. J. Winzer, D. T. Neilson, and A. R. Chraplyvy, Fiber-optic transmission and networking: The previous 20 and the next 20 years, *Opt. Express* **26**, 24190 (2018).
- [29] M. Sibley, *Optical Communications*, 3rd ed. (Springer, Cham, 2020)
- [30] H. J. McGuinness, M. G. Raymer, C. J. McKinstrie, and S. Radic, Quantum Frequency Translation of Single-Photon States in a Photonic Crystal Fiber, *Phys. Rev. Lett.* **105**, 093604 (2010).
- [31] S. Zaske, A. Lenhard, C. A. Keßler, J. Kettler, C. Hepp, C. Arend, R. Albrecht, W.-M. Schulz, M. Jetter, P. Michler, and C. Becher, Visible-to-Telecom Quantum Frequency Conversion of Light from a Single Quantum Emitter, *Phys. Rev. Lett.* **109**, 147404 (2012).
- [32] J. Kim, R. Clark, and D. Gauthier, Low-noise frequency downconversion for long-distance distribution of entangled atomic qubits, in *2013 IEEE Photonics Society Summer Topical Meeting Series* (IEEE, Piscataway, NJ, 2013), pp. 183–184.
- [33] S. Kasture, F. Lenzini, B. Haylock, A. Boes, A. Mitchell, E. W. Streed, and M. Lobino, Frequency conversion between UV and telecom wavelengths in a lithium niobate waveguide for quantum communication with Yb<sup>+</sup> trapped ions, *J. Opt.* **18**, 104007 (2016).
- [34] B. Kambs, J. Kettler, M. Bock, J. N. Becker, C. Arend, A. Lenhard, S. L. Portalupi, M. Jetter, P. Michler, and C. Becher, Low-noise quantum frequency down-conversion of indistinguishable photons, *Opt. Express* **24**, 22250 (2016).
- [35] J. D. Siverns, X. Li, and Q. Quraishi, Ion-photon entanglement and quantum frequency conversion with trapped Ba<sup>+</sup> ions, *Appl. Opt.* **56**, B222 (2017).
- [36] H. Rütz, K.-H. Luo, H. Suche, and C. Silberhorn, Quantum frequency conversion between infrared and ultraviolet, *Phys. Rev. Appl.* **7**, 024021 (2017).
- [37] M. Bock, P. Eich, S. Kucera, M. Kreis, A. Lenhard, C. Becher, and J. Eschner, High-fidelity entanglement between a trapped ion and a telecom photon via quantum frequency conversion, *Nat. Commun.* **9**, 1998 (2018).
- [38] M. Meraner, A. Mazloom, V. Krutyanskiy, V. Krcmarsky, J. Schupp, D. A. Fioretto, P. Sekatski, T. E. Northup, N. Sangouard, and B. P. Lanyon, Indistinguishable photons from a trapped-ion quantum network node, *Phys. Rev. A* **102**, 052614 (2020).
- [39] J. Hannegan, U. Saha, J. D. Siverns, J. Cassell, E. Waks, and Q. Quraishi, C-band single photons from a trapped ion via two-stage frequency conversion, *Appl. Phys. Lett.* **119**, 084001 (2021).
- [40] U. I. Safronova and M. S. Safronova, Relativistic many-body calculation of energies, transition rates, lifetimes, and multipole polarizabilities in Cs-like La III, *Phys. Rev. A* **89**, 052515 (2014).
- [41] J. R. de Laeter, J. K. Böhlke, P. De Bièvre, H. Hidaka, H. S. Peiser, K. J. R. Rosman, and P. D. P. Taylor, Atomic weights of the elements: Review 2000 (IUPAC technical report), *Pure Appl. Chem.* **75**, 683 (2003).
- [42] S. Olmschenk, P. R. Banner, J. Hankes, and A. M. Nelson, Optogalvanic spectroscopy of the hyperfine structure of the  $5p^65d^2D_{3/2,5/2}$  and  $5p^64f^2F_{5/2,7/2}^o$  levels of La III, *Phys. Rev. A* **96**, 032502 (2017).
- [43] F. Li, H. Ma, and Y.-B. Tang, Relativistic coupled-cluster calculation of hyperfine-structure constants of La<sup>2+</sup>, *J. Phys. B: At., Mol. Opt. Phys.* **54**, 065003 (2021).
- [44] A. Kramida, Y. Ralchenko, J. Reader, and NIST ASD Team, NIST Atomic Spectra Database (ver. 5.8), [Online]. Available: <https://physics.nist.gov/asd> [2021, August 24]. National Institute of Standards and Technology, Gaithersburg, MD (2020).
- [45] S. Urabe, M. Watanabe, H. Imajo, and K. Hayasaka, Laser cooling of trapped Ca<sup>+</sup> and measurement of the  $3^2D_{5/2}$  state lifetime, *Opt. Lett.* **17**, 1140 (1992).
- [46] A. A. Madej and J. D. Sankey, Single, trapped Sr<sup>+</sup> atom: Laser cooling and quantum jumps by means of the  $4d^2D_{5/2} - 5s^2S_{1/2}$  transition, *Opt. Lett.* **15**, 634 (1990).
- [47] W. Neuhauser, M. Hohenstatt, P. Toschek, and H. Dehmelt, Optical-Sideband Cooling of Visible Atom Cloud Confined in Parabolic Well, *Phys. Rev. Lett.* **41**, 233 (1978).
- [48] H. R. Gray, R. M. Whitley, and C. R. Stroud, Coherent trapping of atomic populations, *Opt. Lett.* **3**, 218 (1978).
- [49] A. S. Bell, P. Gill, H. A. Klein, A. P. Levick, C. Tamm, and D. Schnier, Laser cooling of trapped ytterbium ions using a four-level optical-excitation scheme, *Phys. Rev. A* **44**, R20(R) (1991).
- [50] S. Olmschenk, K. C. Younge, D. L. Moehring, D. N. Matsukevich, P. Maunz, and C. Monroe, Manipulation and detection of a trapped Yb<sup>+</sup> hyperfine qubit, *Phys. Rev. A* **76**, 052314 (2007).
- [51] R. Ozeri, The trapped-ion qubit tool box, *Contemp. Phys.* **52**, 531 (2011).
- [52] J. Benhelm, G. Kirchmair, C. F. Roos, and R. Blatt, Experimental quantum-information processing with <sup>43</sup>Ca<sup>+</sup> ions, *Phys. Rev. A* **77**, 062306 (2008).
- [53] E. Arimondo, M. Inguscio, and P. Violino, Experimental determinations of the hyperfine structure in the alkali atoms, *Rev. Mod. Phys.* **49**, 31 (1977).
- [54] D. J. Wineland, C. Monroe, W. M. Itano, D. Leibfried, B. E. King, and D. M. Meekhof, Experimental issues in coherent quantum-state manipulation of trapped atomic ions, *J. Res. Natl. Inst. Stand. Technol.* **103**, 259 (1998).
- [55] M. Acton, K.-A. Brickman, P. C. Haljan, P. J. Lee, L. Deslauriers, and C. Monroe, Near-perfect simultaneous measurement of a qubit register, *Quantum Inf. Comput.* **6**, 465 (2006).
- [56] C. E. Langer, High fidelity quantum information processing with trapped ions, Ph.D. thesis, University of Colorado at Boulder, 2006.
- [57] R. Noek, G. Vrijsen, D. Gaultney, E. Mount, T. Kim, P. Maunz, and J. Kim, High speed, high fidelity detection of an atomic hyperfine qubit, *Opt. Lett.* **38**, 4735 (2013).
- [58] R. Maiwald, A. Golla, M. Fischer, M. Bader, S. Heugel, B. Chalopin, M. Sondermann, and G. Leuchs, Collecting more than half the fluorescence photons from a single ion, *Phys. Rev. A* **86**, 043431 (2012).

- [59] C.-K. Chou, C. Aughter, J. Lilieholm, K. Smith, and B. Blinov, Note: Single ion imaging and fluorescence collection with a parabolic mirror trap, *Rev. Sci. Instrum.* **88**, 086101 (2017).
- [60] M. Ghadimi, V. Blüms, B. G. Norton, P. M. Fisher, S. C. Connell, J. M. Amini, C. Volin, H. Hayden, C. S. Pai, D. Kielpinski, M. Lobino, and E. W. Streed, Scalable ion-photon quantum interface based on integrated diffractive mirrors, *npj Quantum Inf.* **3**, 4 (2017).
- [61] C. Crocker, M. Lichtman, K. Sosnova, A. Carter, S. Scarano, and C. Monroe, High purity single photons entangled with an atomic qubit, *Opt. Express* **27**, 28143 (2019).
- [62] G. Araneda, G. Cerchiari, D. B. Higginbottom, P. C. Holz, K. Lakhmanskii, P. Obšil, Y. Colombe, and R. Blatt, The panopticon device: An integrated Paul-trap-hemispherical mirror system for quantum optics, *Rev. Sci. Instrum.* **91**, 113201 (2020).
- [63] T. Walker, S. V. Kashanian, T. Ward, and M. Keller, Improving the indistinguishability of single photons from an ion-cavity system, *Phys. Rev. A* **102**, 032616 (2020).
- [64] H. Takahashi, E. Kassa, C. Christoforou, and M. Keller, Strong Coupling of a Single Ion to an Optical Cavity, *Phys. Rev. Lett.* **124**, 013602 (2020).
- [65] J. Schupp, V. Krcmarsky, V. Krutyanskiy, M. Meraner, T. E. Northup, and B. P. Lanyon, Interface between trapped-ion qubits and traveling photons with close-to-optimal efficiency, *PRX Quantum* **2**, 020331 (2021).
- [66] P. Kobel, M. Breyer, and M. Köhl, Deterministic spin-photon entanglement from a trapped ion in a fiber Fabry-Perot cavity, *npj Quantum Inf.* **7**, 6 (2021).
- [67] B. B. Blinov, D. L. Moehring, L.-M. Duan, and C. Monroe, Observation of entanglement between a single trapped atom and a single photon, *Nature (London)* **428**, 153 (2004).
- [68] D. L. Moehring, M. J. Madsen, K. C. Younge, R. N. Kohn, Jr., P. Maunz, B. B. Blinov, L.-M. Duan, and C. Monroe, Quantum networking with photons and trapped atoms, *J. Opt. Soc. Am. B* **24**, 300 (2007).
- [69] L. Luo, D. Hayes, T. A. Manning, D. N. Matsukevich, P. Maunz, S. Olmschenk, J. D. Sterk, and C. Monroe, Protocols and techniques for a scalable atom-photon quantum network, *Fortschr. Phys.* **57**, 1133 (2009).
- [70] T. Kim, P. Maunz, and J. Kim, Efficient collection of single photons emitted from a trapped ion into a single-mode fiber for scalable quantum-information processing, *Phys. Rev. A* **84**, 063423 (2011).
- [71] L.-M. Duan, M. J. Madsen, D. L. Moehring, P. Maunz, R. N. Kohn, Jr., and C. Monroe, Probabilistic quantum gates between remote atoms through interference of optical frequency qubits, *Phys. Rev. A* **73**, 062324 (2006).
- [72] S. C. Connell, J. Scarabel, E. M. Bridge, K. Shimizu, V. Blüms, M. Ghadimi, M. Lobino, and E. W. Streed, Ion-photon frequency qubit correlations for quantum networks, *J. Phys. B: At., Mol. Opt. Phys.* **54**, 175503 (2021).
- [73] P. Maunz, S. Olmschenk, D. Hayes, D. N. Matsukevich, L.-M. Duan, and C. Monroe, Heralded Quantum Gate between Remote Quantum Memories, *Phys. Rev. Lett.* **102**, 250502 (2009).
- [74] J. Brendel, N. Gisin, W. Tittel, and H. Zbinden, Pulsed Energy-Time Entangled Twin-Photon Source for Quantum Communication, *Phys. Rev. Lett.* **82**, 2594 (1999).
- [75] S. D. Barrett and P. Kok, Efficient high-fidelity quantum computation using matter qubits and linear optics, *Phys. Rev. A* **71**, 060310(R) (2005).
- [76] H. Bernien, B. Hensen, W. Pfaff, G. Koolstra, M. S. Blok, L. Robledo, T. H. Taminiau, M. Markham, D. J. Twitchen, L. Childress, and R. Hanson, Heralded entanglement between solid-state qubits separated by three metres, *Nature (London)* **497**, 86 (2013).
- [77] Based on SMF-28 Ultra optical fiber specification for max attenuation  $\leq 0.32$  dB/km at the 1383 nm water absorption peak.
- [78] Corning® SMF-28® Ultra Optical Fiber (Corning Inc., New York, 2019).
- [79] C. Monroe, R. Raussendorf, A. Ruthven, K. R. Brown, P. Maunz, L.-M. Duan, and J. Kim, Large-scale modular quantum-computer architecture with atomic memory and photonic interconnects, *Phys. Rev. A* **89**, 022317 (2014).
- [80] S. Santra, S. Muralidharan, M. Lichtman, L. Jiang, C. Monroe, and V. S. Malinovskiy, Quantum repeaters based on two species trapped ions, *New J. Phys.* **21**, 073002 (2019).
- [81] Q. A. Turchette, D. Kielpinski, B. E. King, D. Leibfried, D. M. Meekhof, C. J. Myatt, M. A. Rowe, C. A. Sackett, C. S. Wood, W. M. Itano, C. Monroe, and D. J. Wineland, Heating of trapped ions from the quantum ground state, *Phys. Rev. A* **61**, 063418 (2000).
- [82] M. Brownnutt, M. Kumph, P. Rabl, and R. Blatt, Ion-trap measurements of electric-field noise near surfaces, *Rev. Mod. Phys.* **87**, 1419 (2015).
- [83] H. Häffner, C. F. Roos, and R. Blatt, Quantum computing with trapped ions, *Phys. Rep.* **469**, 155 (2008).
- [84] V. Krutyanskiy, M. Meraner, J. Schupp, V. Krcmarsky, H. Hainzer, and B. P. Lanyon, Light-matter entanglement over 50 km of optical fibre, *npj Quantum Inf.* **5**, 72 (2019).
- [85] This estimate of the distance-limited rate assumes  $c$  as the speed of the quantum signal (photon) and  $c/2$  as the speed of the classical detection signal, yielding a total time duration  $t = L/c + L/(c/2) = 3L/c$ . For a distance  $L$  of about 5 km,  $t = 50\mu\text{s}$ , which is already more than  $10\times$  the excited state lifetime.
- [86] K. R. Brown, J. Kim, and C. Monroe, Co-designing a scalable quantum computer with trapped atomic ions, *npj Quantum Inf.* **2**, 16034 (2016).
- [87] P. Dhara, N. M. Linke, E. Waks, S. Guha, and K. P. Seshadreesan, Multiplexed quantum repeaters based on dual-species trapped-ion systems, *Phys. Rev. A* **105**, 022623 (2022).
- [88] D. Kielpinski, B. E. King, C. J. Myatt, C. A. Sackett, Q. A. Turchette, W. M. Itano, C. Monroe, D. J. Wineland, and W. H. Zurek, Sympathetic cooling of trapped ions for quantum logic, *Phys. Rev. A* **61**, 032310 (2000).
- [89] J. P. Home, D. Hanneke, J. D. Jost, J. M. Amini, D. Leibfried, and D. J. Wineland, Complete methods set for scalable ion trap quantum information processing, *Science* **325**, 1227 (2009).
- [90] B. Lekitsch, S. Weidt, A. G. Fowler, K. Mølmer, S. J. Devitt, C. Wunderlich, and W. K. Hensinger, Blueprint for a microwave trapped ion quantum computer, *Sci. Adv.* **3**, e1601540 (2017).
- [91] M. Raghunandan, F. Wolf, C. Ospelkaus, P. O. Schmidt, and H. Weimer, Initialization of quantum simulators by sympathetic cooling, *Sci. Adv.* **6**, eaaw9268 (2020).
- [92] A. B. Klimov, R. Guzmán, J. C. Retamal, and C. Saavedra, Qutrit quantum computer with trapped ions, *Phys. Rev. A* **67**, 062313 (2003).

- [93] C. Senko, P. Richerme, J. Smith, A. Lee, I. Cohen, A. Retzker, and C. Monroe, Realization of a Quantum Integer-Spin Chain with Controllable Interactions, *Phys. Rev. X* **5**, 021026 (2015).
- [94] J. Randall, S. Weidt, E. D. Standing, K. Lake, S. C. Webster, D. F. Murgia, T. Navickas, K. Roth, and W. K. Hensinger, Efficient preparation and detection of microwave dressed-state qubits and qutrits with trapped ions, *Phys. Rev. A* **91**, 012322 (2015).
- [95] F. M. Leupold, M. Malinowski, C. Zhang, V. Negnevitsky, A. Cabello, J. Alonso, and J. P. Home, Sustained State-Independent Quantum Contextual Correlations from a Single Ion, *Phys. Rev. Lett.* **120**, 180401 (2018).
- [96] P. J. Low, B. M. White, A. A. Cox, M. L. Day, and C. Senko, Practical trapped-ion protocols for universal qudit-based quantum computing, *Phys. Rev. Res.* **2**, 033128 (2020).